

Temporal Convolutional Autoencoder for Interference Mitigation in FMCW Radar Altimeters

Charles E. Thornton*, Jamie Sloop*, Samuel Brown*, Aaron Orndorff*, William C. Headley*, Stephen Young†

*Virginia Tech National Security Institute, Blacksburg, VA, USA

†The Boeing Company, Crystal City, VA, USA

Abstract—We investigate the end-to-end altitude estimation performance of a convolutional autoencoder-based interference mitigation approach for frequency-modulated continuous-wave (FMCW) radar altimeters. Specifically, we show that a Temporal Convolutional Network (TCN) autoencoder effectively exploits temporal correlations in the received signal, providing superior interference suppression compared to a Least Mean Squares (LMS) adaptive filter. Unlike existing approaches, the present method operates directly on the received FMCW signal. Additionally, we identify key challenges in applying deep learning to wideband FMCW interference mitigation and outline directions for future research to enhance real-time feasibility and generalization to arbitrary interference conditions.

Index Terms—interference mitigation, radar signal processing, radio frequency machine learning, autoencoder

I. INTRODUCTION AND MOTIVATION

Precise and reliable altitude measurements are essential in a number of airborne applications. Radar altimeters are widely employed to obtain such measurements for objectives such as commercial aviation, the operation of unmanned aerial systems, and military missions at low altitudes. Due to the sensitive nature of these and related applications, it is crucial to understand all potential sources of system failure and performance degradation.

A particularly notable threat to reliable radar altimeter operation is radio-frequency (RF) interference from neighboring systems, which could be either intentional or incidental. Commercial altimeters commonly operate in the 4.2–4.4 GHz band, which has created concern among regulators given the increased proliferation of communication systems in the 1–6 GHz spectrum. For example, in January 2023, the Federal Aviation Administration (FAA) issued a deadline for all commercial airlines to upgrade altimeters to ensure safe operation in the vicinity of 5G C-Band signals.

By September 2023, the entire US airline fleet had updated their altimeter equipment to ensure that the risk of 5G interference would be mitigated through 2027. However, the possibility of interference from other sources, the use of radar altimeters in wider applications, and the growing congestion of the sub 6 GHz spectrum all provide pressing demand for robust interference mitigation strategies in future generations of radar altimeters.

Interference mitigation in radar systems is an important and broad area of research [2]. Conventional approaches

for interference suppression include time-frequency domain techniques such as adaptive filtering, spectral masking, and wavelet-based methods. In addition, antenna-based techniques such as phased array beamforming and null steering may be applied to suppress interference in the spatial domain. Another approach is to detect and cancel interference by monitoring changes in amplitude, frequency, or phase.

In recent years, denoising autoencoders (DAEs) have emerged as a compelling approach for interference mitigation. DAEs learn a compact (low-dimensional) representation of the desired signal during a training process, which allows the learned model to adapt to interference patterns that may be too complex for traditional filters. Additionally, once the model is trained, interference mitigation can be performed by a single forward pass through the model, which may be faster than iterative methods such as adaptive filtering.

However, there are several challenges associated with the use of DAEs for interference mitigation. First, the training data is required to be diverse and representative of dynamic real-world conditions. Second, the training phase can be computationally intensive and may be difficult to scale to wide bandwidth signals. Third, DAEs may be more difficult to interpret than some conventional methods which may pose a difficulty for sensitive applications such as aviation.

A. Contributions

While denoising autoencoders have been previously proposed for radar interference mitigation, our work provides several key contributions:

- 1) Direct processing of received signals: Unlike prior approaches that operate on processed radar data (e.g., range-Doppler images or beat signals), our method directly processes the raw received time-domain signal without requiring prior interference detection or transformation. This makes it more adaptable to real-time applications and diverse interference conditions.
- 2) Temporal modeling with Temporal Convolutional Network (TCN) autoencoders: We develop and validate an efficient TCN autoencoder tailored for radar interference mitigation. Unlike conventional convolutional neural network (CNN) autoencoders, the TCN architecture explicitly accounts for strong temporal correlations in FMCW radar signals, improving interference suppression performance.

Portions of this work were presented at IEEE MILCOM 2024, Washington DC, USA [1].

- 3) Comprehensive Performance Evaluation: We systematically evaluate the TCN autoencoder within an end-to-end radar altimeter simulation environment, benchmarking its effectiveness against Least Mean Squares (LMS) adaptive filtering and baseline processing. This comparison provides insights into the general trade-offs between adaptive filtering and deep learning-based denoising approaches.
- 4) Real-Time Implementation Feasibility: We demonstrate the practicality of the TCN-based approach for real-time hardware deployment, highlighting its efficiency in handling sequential radar data and its suitability for embedded systems.

II. PRIOR ART

The general topic of radar interference mitigation has been extensively explored, but remains continually relevant due to its practical importance. An important survey of recent techniques is provided in [2]. For the particular case of FMCW radar, [3] applies a distributed networking protocol that coordinates FMCW radar transmission among vehicles, and demonstrate the necessity of coordination or interference mitigation in RF dense environments.

For radar altimeters, [4] discusses simulation tools for radar system modeling, particularly for airborne radar altimeters. The focus is on electromagnetic wave propagation modeling, including the impact of terrain and environmental conditions. It highlights how ray-tracing and full-wave solvers can be used to evaluate altimeter performance and interference effects in complex environments. In [5] industry standards and regulatory guidelines for radar altimeter performance and certification. It outlines requirements for altimeter operation in shared spectrum environments, ensuring resilience against interference from communication systems. Amaireh *et al.* [6] explore machine learning-based approaches for radar altimeter signal processing. Rock *et al.* (2024) [7] investigate deep learning-based interference mitigation for radar altimeters. The work presents a CNN autoencoder designed to suppress interference from adjacent frequency bands, including 5G signals.

Autoencoders have been previously used to extract features and denoise radar signals. Kokalj-Filipovic *et al.* [8] demonstrate the effectiveness of autoencoders in training compact deep learning classifiers for wireless protocols, using multiple denoising autoencoders to extract features for RF signal classification. In [9], a convolutional autoencoder is applied for interference mitigation; however, the model operates on range-Doppler images rather than directly on the time-domain received signal, which may result in a loss of information. Chen *et al.* [10], apply a CNN-based autoencoder with gated convolutions to the beat (intermediate frequency) signal for automotive radar interference mitigation. However, this approach requires a prior detection of interference-contaminated samples before the denoising operation, whereas the approach in this paper operates directly on the received time-domain signal without a prior detection step.

TCNs are a network architecture designed to capture temporal relationships across multiple time scales, including low, intermediate, and high-level temporal features [11]. Because they use fewer connections than traditional CNNs, TCNs can be trained more quickly while leveraging temporal correlations to improve performance. Chauhan *et al.* have investigated the TCN architecture in a range of applications, including speech recognition, anomaly detection, landslide displacement prediction, malware detection, and traffic flow forecasting [12]. Their work highlights several advantages of TCNs, such as parallel data processing, adaptable model design, effective use of dilated convolutions to mitigate gradient issues, and the ability to process inputs of variable length, a limitation often encountered in conventional CNNs. In addition, Park *et al.* propose combining TCNs with autoencoder models to overcome the challenges faced by recurrent autoencoders when modeling time series data, particularly the information bottleneck associated with fixed-length vectors [13]. Their findings suggest that temporal convolutional autoencoders outperform baseline models on real-world, temporally correlated data.

In addition to recent deep learning approaches, traditional interference mitigation strategies for radar have been widely studied. Griffiths *et al.* [14] provide a comprehensive overview of spectrum engineering and regulatory challenges associated with radar coexistence in congested environments. Uysal and Sanka [15] demonstrate interference suppression for automotive radar using time-frequency techniques, which remain relevant benchmarks for assessing the performance of machine learning-based methods. These works highlight the ongoing need for robust and adaptable interference mitigation in radar systems, particularly as spectral congestion increases.

III. RADAR ALTIMETER SYSTEM MODEL

We consider a radar altimeter operating at center frequency f_c , assumed to be in the 4.2-4.4GHz band, and occupying bandwidth B . The altimeter takes measurements over a series of discrete time steps $k = 1, 2, \dots, n$. During each time step, the radar transmits a triangular sweep FMCW signal expressed by

$$S_T(t) = A_{tx} \cos \left(2\pi \left(f_c t + \frac{\alpha}{2} \text{sign}(t) T_{\text{fold}}^2(t) \right) \right), \quad (1)$$

over the interval $t \in [-T_{sw}/2, T_{sw}/2]$, where T_{sw} is the sweep time. In (1), we define

$$\text{sign} = (-1)^{\lfloor \frac{t \bmod T_{sw}}{T_{sw}/2} \rfloor}, \quad (2)$$

A_{tx} is the amplitude, α is the sweep rate in Hz/s, and

$$T_{\text{fold}} = (t \bmod T_{sw}) \bmod \frac{T_{sw}}{2}. \quad (3)$$

Then, the received signal can be written as

$$S_R(t) = S_{\text{target}}(t) + S_{\text{intf}}(t) + S_{\text{clutter}}(t) + n(t), \quad (4)$$

where

$$S_{\text{target}}(t) = A_{rx} \cos \left(2\pi \left(f_c(t - \tau) + \frac{\alpha}{2} \text{sign}(t - \tau) T_{\text{fold}}^2(t - \tau) \right) - \phi_D \right), \quad (5)$$

is the return from the ground at a delay of τ and a Doppler shift of ϕ_D . Similarly, the clutter return $S_{\text{clutter}}(t)$ consists of a sum of additional returns from the land surface, obstacles, and other scatterers at various delays and Doppler shifts. The terms $S_{\text{intr}}(t)$ and $n(t)$ express unwanted noise due to external interference and other physical factors, respectively.

To generate a profile of range responses from the received FMCW signal, $S_R(t)$, a conventional beat frequency extraction process is employed using an FFT dechirping method. Since the FMCW signal consists of both upsweep and downsweep components, the received signal is split into upsweep and downsweep components, and mixed with reference signals, which consist of the respective upsweep and downsweep portions of the transmitted signal. Cell-averaging constant false alarm rate (CA-CFAR) detection is then used to obtain range estimates from the upsweep and downsweep range profiles. These range estimates are averaged to obtain an estimate of the aircraft's altitude.

To improve the quality of altitude measurements, we seek primarily to remove the unwanted additive interference in the received signal, as well as noise and clutter components to the degree possible. For this purpose, we apply the convolutional autoencoder described in the next section. The trained autoencoder takes $S_R(t)$ as an input and produces a denoised reconstruction $S_{R,\text{Clean}}(t)$ as an output.

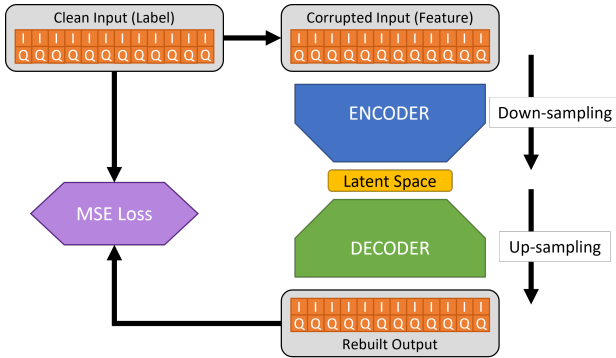


Fig. 1: High-level diagram of denoising autoencoder operation on received IQ data.

IV. TEMPORAL CONVOLUTIONAL AUTOENCODER MODEL AND TRAINING

A. Model Architecture

The model architecture presented in this work uses an autoencoder structure in which the dimensionality of the input space is reduced to form a latent representation before expanding again to form an output space with the same dimension as the input space. This compression step forces the model to generalize the patterns in the feature space while discarding most of the information. The autoencoder structure, often referred to as a bottleneck, is designed to perform a denoising operation on the inputs by removing unwanted information; i.e., nuisance parameters, and preserving the desired patterns in the feature space. The application of this autoencoder to RF

signal processing introduces several non-traditional requirements, such as the ability to handle complex-valued inputs and outputs. There are multiple techniques for incorporating complex data into existing neural network architectures of which there are two main categories; those utilizing complex weights and biases, and those using only real weights and biases. The chosen technique for this model divides real and imaginary parts into separate channels such that the input signals have dimensions $N \times 2$ and subsequently applies 1D convolution operations, the first convolution naturally mixing the IQ components and reducing the signal to a 1D sample vector. Although an alternative approach exists where the magnitude and phase of the signal are used instead of the real and imaginary components, the two-channel IQ format has been shown through this AEC architecture to be capable of adequately preserving the frequency/phase relationships of the input signal.

The denoising and interference mitigation capabilities of the AEC are made possible through the bottleneck structure which forces generalization on certain features and discarding of extraneous information, hopefully corresponding to the interference to be removed. The amount by which the dimensionality of the input signal is reduced in the latent representation is referred to as the compression ratio. Obtaining the optimal compression ratio is one of the main considerations driving the AEC design.

Building on preliminary work [1], which explored CNN and fully connected (FC) autoencoders, we developed a TCN-based architecture that provides enhanced temporal feature extraction while reducing model complexity.

Our preliminary work compared a CNN-only model with an FC model. We observed that the CNN model outperformed the FC model in most scenarios and trained faster because of its reduced connectivity. Since then, we have expanded our evaluation to include a TCN. For these comparisons, each model was trained on a dataset of 50,000 signals, which is lower than the amount of data typically used for optimal performance. The dataset contained signals with tone-based, QPSK, and 5G interference. We evaluated the models both quantitatively by measuring the root-mean-square error (RMSE) between the predicted and clean signals and qualitatively by visually comparing the Short-Time Fourier Transform (STFT) of the output signals with those of the input and the training label. Although the FC and CNN models produced similar STFTs, there were differences in the RMSE of their output, with the CNN model performing better. The reconstructed signals showed visibly reduced interference artifacts in the STFT, along with improved beat signal clarity for range estimation. Figure 3 shows the STFT results side by side, including the input signals and the clean evaluation labels, followed by the output of each AEC model for 5 different evaluation examples.

To break down our design choices further, we employ several strategies to enhance feature extraction and maintain robust performance. The ReLU activation functions introduce non-linearity into the network, enabling it to model complex relationships that purely linear operations cannot capture. After

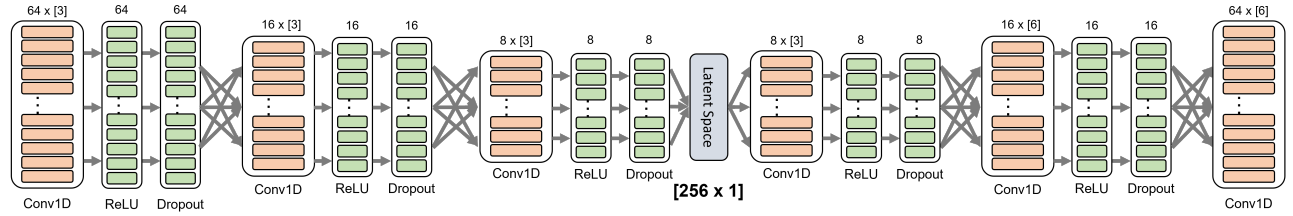


Fig. 2: Diagram of TCN Autoencoder Model Architecture. The model uses dilated convolutions to expand the receptive field without reducing temporal resolution. Dimensionality reduction is achieved via the latent bottleneck, transpose convolution stride is used in the decoder to efficiently upsample the latent representation to the original signal length, a rectified linear unit function is used to introduce nonlinearity, and dropout for regularization.

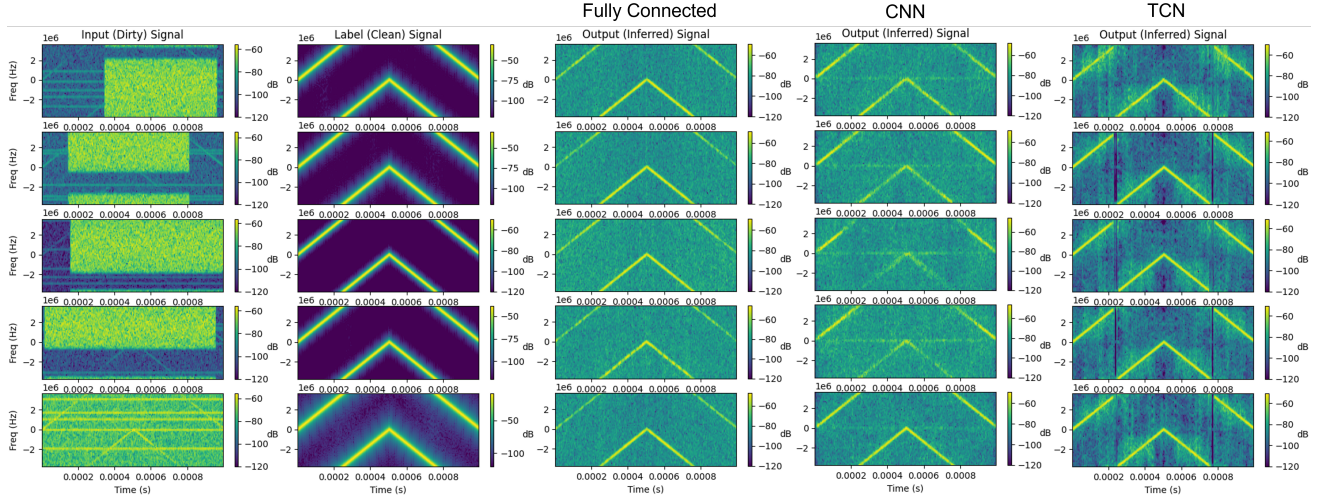


Fig. 3: Model Comparison. Comparison of STFTs for the input signal, reference signal, and the output of each of the three models. Each row shows a different evaluation example from the dataset, combining QPSK and tone interference.

each convolution, dropout layers randomly disable neurons during training, helping to prevent overfitting and promoting the learning of generalizable features. Additionally, dilated convolutions effectively ‘stretch’ the receptive field, allowing the model to capture long-range temporal dependencies in the RF signals without a significant increase in parameters. Finally, the stride parameter is carefully chosen to balance detail preservation and computational efficiency: in the encoder, a stride of 1 is used to capture every temporal detail, whereas, in the decoder, higher strides in the transpose convolutions efficiently upsample the latent representation to reconstruct the input signal’s resolution.

The new TCN model inherently mixes the IQ components within its initial 1D convolution operations and leverages dilated convolutions for improved temporal correlation capture. This approach simplifies the overall architecture, reduces parameter overhead, and better preserves the critical frequency and phase relationships of the input signal. These benefits, along with faster training times, make the TCN architecture particularly well-suited for processing large-scale RF signals. In the following sections, we describe the detailed design of the TCN-based AEC, highlighting its streamlined structure, hyper-parameters, and performance benefits over our previous

implementations.

The primary distinction in the design of this AEC architecture now lies in its use of a TCN-based design that relies exclusively on 1D convolution operations, rather than the CNN layers previously compared to fully-connected layers. The TCN design achieves a compact latent representation by combining dilated convolutions and a fully connected bottleneck layer, requiring fewer parameters than fully connected or CNN-based autoencoders. While fully connected layers can perform dimensionality reduction by simply reducing subsequent layer sizes, they incur a high parameter cost when handling large sample-length inputs. In contrast, 1D convolution layers in the TCN AEC achieve dimensionality reduction by employing carefully selected strides and dilated convolutions, with parameter requirements depending on kernel size and the number of channels. This strategy enables efficient compression even for large signals without ballooning memory and computational needs.

The AEC model architecture is depicted in Figure 2, highlighting the chosen structure and hyper-parameters. The final TCN autoencoder architecture consists of a 1D convolutional encoder and a mirrored transpose-convolutional decoder. The input to the model is a complex-valued IQ signal of length

7500 samples, represented as two real-valued channels (real and imaginary), resulting in an input shape of (7500, 2). The encoder comprises three 1D convolutional layers with kernel size 3, stride 1, and padding 2. These layers use dilation factors of 1, 2, and 4, respectively, and have 128, 64, and 32 output channels. Each convolutional layer is followed by a ReLU activation. The output is then flattened and passed through a fully connected layer to produce a 128-dimensional latent representation. The use of increasing dilation factors allows the encoder to capture long-range temporal dependencies without increasing model depth or reducing resolution. Importantly, no pooling is used, and the stride is fixed at 1 throughout the encoder to preserve temporal structure.

The decoder mirrors this structure. A fully connected layer first projects the 128-dimensional latent vector to a tensor of shape (32, 117), which is reshaped and passed through three 1D transpose convolutional layers. These layers upsample the signal with the following configurations: 32 to 64 channels (kernel size 3, stride 3), 64 to 128 channels (kernel size 6, stride 5), and 128 to 2 channels (kernel size 6, stride 5). A final linear interpolation layer ensures the output matches the original input length of 7500 samples per channel. The total number of learnable parameters in the model is approximately 920,000. This architecture balances expressive capacity with computational efficiency, enabling deployment in real-time radar altimeter systems.

TABLE I: TCN AEC Model Parameters

Layer	Kernel Size	Stride	Padding	Dilation
1	3	1	2	1
2	3	1	2	2
3	3	1	2	4
4	3	3	1	1
5	6	5	1	1
6	6	5	1	1

The loss function employed for the AEC compares the rebuilt inferred output signals to the clean label signals using L2 loss (or mean-square-error). The loss function compares the raw signals which allows for optimization over the full signal dimension.

B. Model Training

The TCN autoencoder was trained on 10,000 complex-valued FMCW radar signals, each consisting of 7500 IQ samples, with an additional 1,000 examples reserved for validation. Prior to training, the real and imaginary components of each sample were normalized independently to unit peak amplitude. These normalized values were then treated as two separate input channels. Training was performed using the Adam optimizer with a fixed learning rate of 0.001 and a mean squared error (MSE) loss function. The model was trained for 150 epochs using a batch size of 128. Training and validation were performed on an NVIDIA GPU using PyTorch.

Evaluation metrics included both the root-mean-square error (RMSE) between reconstructed and clean signals, and the

accuracy of the resulting altitude estimates after processing by the radar altimeter signal chain. Compared to prior CNN and fully-connected architectures, the TCN autoencoder trained more quickly per epoch and achieved lower RMSE and more accurate range detection. The reduced parameter count and ability to model long-range correlations made the TCN particularly well-suited for denoising in the radar altimeter setting.

The amplitude variation was applied to vary the envelope of the FMCW signals in a manner similar to the effect of constructive and destructive interference from a multipath fading channel. The radar signal envelope was varied using a band-limited Gaussian process to simulate the amplitude fluctuations caused by multipath fading via a band-limited Gaussian process having 10% of the bandwidth of the FMCW signal and a standard deviation of 0.3. The Gaussian noise was then added to set the SNR level for the radar altimeter in the range [-25, 30] dB. Interference was added through some combination of tones, QPSK, and 5G signals. Tones were spaced uniformly in frequency across the FMCW bandwidth and had SIR values in the range [-20, 20] dB. The QPSK interference was meant to mimic communications signals spanning some portion of the radar bandwidth and pulse duration, with bandwidths and durations uniformly spaced across frequency and time and SIR values in the range [-20, 0] dB. To simulate 5G interference, we generated a downlink FRC waveform using key parameters such as a variable channel bandwidth (either 5 or 10 MHz), a subcarrier spacing of 15 kHz, and a sample rate of 7.5 MHz. This waveform, spanning 10 subframes and incorporating standard elements like synchronization bursts, control resource sets, and a full-band QPSK-modulated PDSCH, closely mimics the dynamic characteristics of a real 5G downlink signal.

The process employed for model refinement and hyperparameter tuning involved training the model on smaller 7500-length signal datasets of 50,000 examples and observing the performance in terms of rebuilt signal quality, range profile peak-to-sidelobe ratios, and range estimation accuracy. Figure 4 illustrates the process used for the evaluation of the model in which inference was made on an evaluation data set created in a similar way to the training data set. Stretch processing is performed on both the inputs and outputs of the AEC using a pre-transmission reference signal, similar to the operation of the actual altimeter system. The stretch-processed signals contain the same information content as the original signals, but this information is transformed to reflect the range estimation capability. The range profiles feature peaks in both positive and negative frequency due to the upsweep and downsweep portions of the FMCW. The range estimate is obtained by detecting and averaging these two peaks. With this evaluation scheme in place, the effectiveness of each trained model was determined by the peak-to-sidelobe ratios for its range profiles, as well as the precision of its range estimates compared to dirty signals.

The main hyperparameters refined during the training and evaluation process were the size, dilation, and compression

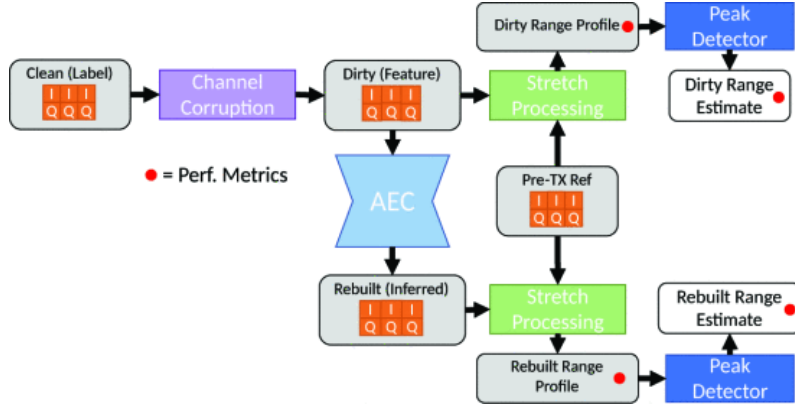


Fig. 4: Range Profile Evaluation Scheme

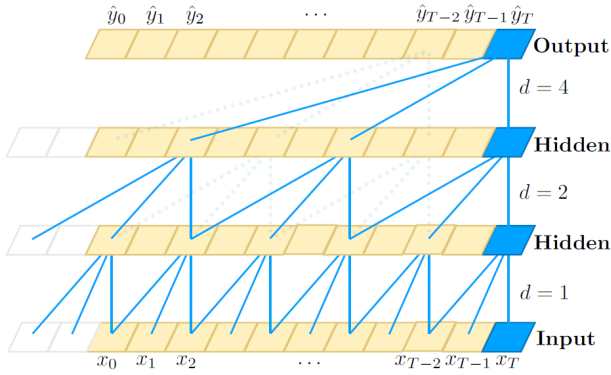


Fig. 5: Conv1D Dilation Visualized [16]

ratio of the TCN kernel. The size of the kernel and the dilation factor have a significant impact on the model's ability to capture and generalize the signal's temporal patterns. In the case of TCNs, the kernel size is typically much smaller than in CNN models. Our TCN model uses a kernel size of 3 to 6 while our previous CNN model used a kernel size of 200. Smaller kernels work effectively in the TCN due to the dilation mechanism, which allows the model to capture long-range dependencies over time without needing larger kernels as shown in Figure 5. The dilation factor, which controls the spacing between kernel elements, was also tuned to optimize the receptive field and allow the model to capture long-term correlations in the signal, even with a small kernel size. In combination, these parameters enable the TCN to generalize well to the shape of the signal while maintaining efficiency.

For the compression ratio, latent space dimensions of around 1.5% to 5% of the input dimension were observed to result in the best performance in terms of MSE. This is smaller than what was found in the CNN model, where a range of 10% to 20% produced the best results. The smaller latent space in the TCN helps retain the essential features of the signal while reducing the amount of unnecessary information, which is beneficial for both generalization and computational efficiency.

Taking these findings into account, the final model architecture emphasizes achieving the optimal compression ratio while accommodating the smaller kernel size required by the TCN. The kernel size of 3 to 6 was selected for each layer, reflecting the benefits of dilation and the need for fewer parameters. The choice of smaller kernel sizes is not only influenced by the model's ability to capture long-range temporal dependencies but also by the computational efficiency gained from using smaller kernels compared to larger ones in traditional CNN architectures.

V. SIMULATION STUDY

The autoencoder (AEC) model is evaluated within a comprehensive simulation of a commercial aircraft radar altimeter system based on the MATLAB FMCW Radar Altimeter Simulation framework [17]. The simulation replicates a realistic landing scenario by integrating real-world data and carefully defined radar parameters as shown in Figure 6. Digital Terrain Elevation Data (DTED) from the United States Geological Survey (USGS) is imported from an actual elevation file, and a set of predefined reflectivity models (such as those based on the APL approach) is available to characterize various land types, for example, Urban, HighRelief, or LowRelief. The DTED Data we use comes from the United State Geological Survey (USGS) group. In our simulation, a low-relief urban setting is selected to represent typical ground conditions. In addition, a real flight trajectory is loaded from a data file to capture an aircraft's approach to Chicago O'Hare Airport. These data sources collectively define the land surface, over which clutter is generated to emulate the range response encountered by the radar altimeter during landing.

The radar altimeter simulation is built upon detailed parameter definitions based on ITU recommendations. Key parameters include a center frequency of 4.3 GHz, a bandwidth of 7.5 MHz, and a frequency of 1000 chirps per second. The system models the altimeter antennas using a phased Gaussian element with a wide beamwidth (approximately 40 degrees) to ensure robust performance despite variations in aircraft attitude. The transmitted waveform is a triangular FMCW signal generated by calculating an appropriate sweep time and

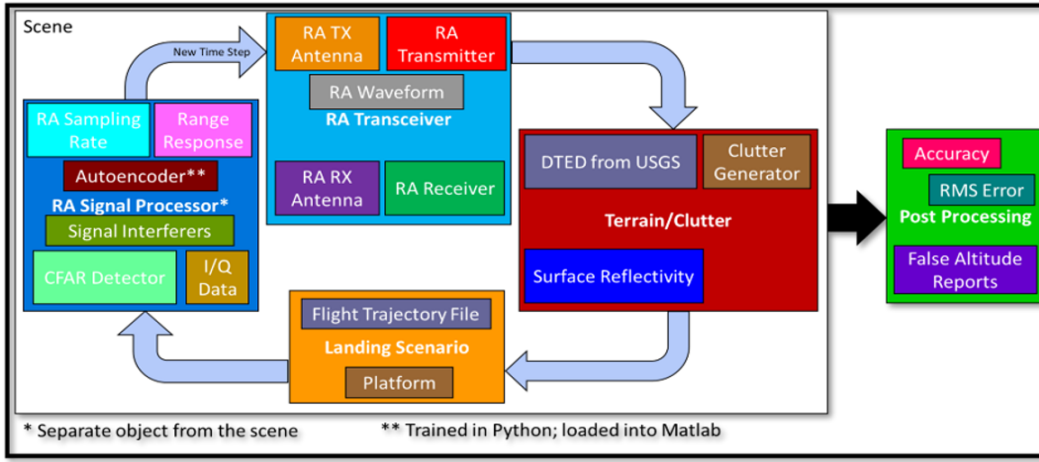


Fig. 6: Altimeter Simulation Diagram

slope. To simulate realistic interference conditions, three types of signals were added to the FMCW radar returns: continuous tones, QPSK-modulated bursts, and a 5G downlink waveform. Continuous wave (CW) tones were placed at uniformly spaced frequencies across the radar bandwidth, with the number of tones and their power levels randomized per example. QPSK interference was generated as short-duration bursts occupying randomly selected time and frequency intervals within the 7500-sample chirp. Each burst mimicked a generic communication signal with randomized bandwidth, duration, and SIR drawn from a uniform range of -20 to 0 dB. The 5G interference was synthesized using a MATLAB NR waveform generator to produce a downlink signal with 15 kHz subcarrier spacing and either 5 or 10 MHz channel bandwidth. This waveform included synchronization, control, and data regions and was aligned to partially overlap the radar chirp in both frequency and time. Overlap refers to the temporal fraction of the 7500-sample FMCW chirp that coincides with the active portion of the interfering signal. All interference signals were combined additively with the FMCW return prior to training and evaluation. The signal-to-interference ratio (SIR) for each example was computed as the ratio of total clean signal power to total interference power, averaged over the 7500-sample input. Interference timing and structure varied per example to encourage model generalization.

As a classical benchmark, we implemented a block LMS adaptive filter using MATLAB's DSP toolbox to process the received signal prior to altitude estimation. The filter was configured with a length of 32, block size of 100, and step size $\mu = 10^{-4}$. The reference signal for adaptation was the clean transmitted chirp, and the filtered output was passed to the altimeter signal processor for range estimation. This baseline served to evaluate the extent to which traditional adaptive filtering could mitigate in-band interference. While the LMS filter achieved moderate performance under low interference overlap, it exhibited significant degradation when the interference duration or power increased, due to limited convergence and mismatch between the interference and reference

signals. Compared to the LMS approach, the TCN autoencoder consistently achieved lower RMSE in reconstructed signals and more accurate altitude estimates, particularly under high-SIR or temporally overlapping interference conditions. For example, At 100% temporal overlap and -15 dB SINR, the TCN reduced RMSE by over 85% relative to the LMS filter.

Two sampling rates are employed: one for generating and dechirping the waveform (based on the signal bandwidth) and a second, lower rate for processing the dechirped beat signal. The radar transceiver component handles both transmission and reception, and its outputs are subsequently fed into a custom altimeter signal processor.

Within the signal processor, the dechirping process, in which the received signal is mixed with the known transmitted waveform, yields a beat frequency that is directly related to the target range. The processor converts these frequency measurements into range values using the known sweep slope and then applies a CFAR (constant false alarm rate) algorithm to detect the ground return from clutter. Detections from both the upsweep and downsweep signals are combined, and the effects of Doppler shift are minimized by averaging to produce a robust altitude estimate. The simulation continuously evaluates performance by comparing the estimated altitude with the true altitude derived from the flight trajectory and terrain data. Plots of range responses, detection results, and altitude error over time provide detailed insights into the altimeter's performance throughout the landing scenario, where varying clutter characteristics and changing beam footprints as the aircraft descends are fully accounted for.

Figure 7 provides a quantitative comparison of range estimation accuracy across different interference mitigation strategies under varying signal-to-interference-plus-noise ratios (SINR) and interference overlap levels. The overlap percentage refers to the fraction of the 7500-sample FMCW chirp that coincides temporally with a QPSK-modulated interfering signal. The RMSE is computed from the altimeter's estimated altitude over a simulated landing scenario. As shown, the raw input (no mitigation) exhibits significant performance degradation

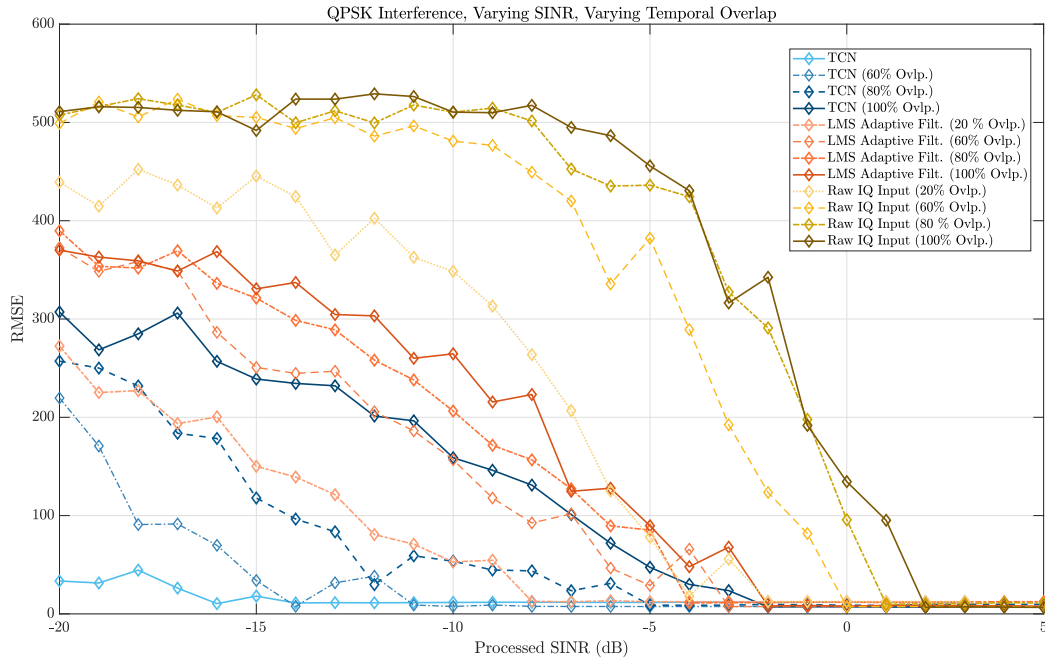


Fig. 7: Root-mean-square error (RMSE) of estimated altitude under QPSK interference for various signal-to-interference-plus-noise ratios (SINR) and temporal overlap levels. Overlap percentages indicate the fraction of the FMCW chirp duration coinciding with the interference burst. The TCN autoencoder maintains low RMSE even under full overlap and low SINR, outperforming both LMS adaptive filtering and unmitigated input. LMS filtering provides modest improvement at partial overlap but degrades significantly at high overlap and low SINR.

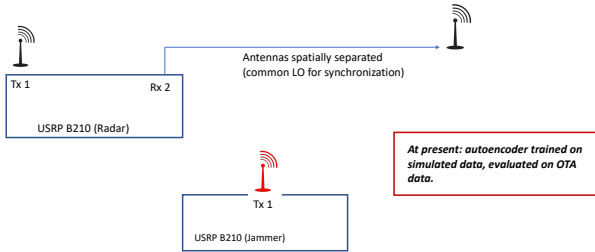


Fig. 8: Over-the-air (OTA) testbed configuration. Two USRP B210 devices transmit radar and interference signals, respectively. A third USRP B210 receives the composite signal. A common local oscillator and spatial antenna separation enable coherent processing. The autoencoder was trained entirely on simulated data and evaluated on these OTA captures.

even under moderate interference, with RMSE exceeding 400 at high overlap and low SINR. The LMS filter improves upon this baseline at partial overlaps but fails to converge effectively at full (100%) interference overlap, particularly below -10 dB SINR. In contrast, the TCN autoencoder maintains robust performance across all overlap levels, achieving RMSE below 50 even under severe conditions (100% overlap at -15 dB SINR). These results highlight the limitations of traditional

adaptive filtering and demonstrate the TCN’s superior ability to learn and suppress structured in-band interference.

These simulation results validate the effectiveness of the TCN autoencoder in mitigating a wide range of interference types under realistic altimeter conditions. Across various terrain types and flight paths, the TCN model demonstrated consistent altitude estimation accuracy and robustness to tone, QPSK, and 5G-style interference. This confirms the model’s practical utility in operational altimeter scenarios.

VI. RESULTS ON OVER-THE-AIR DATA

After training and evaluating our models on MATLAB-generated data, we conducted a quasi real-time evaluation using over-the-air signals. A diagram of the OTA testbed configuration is shown in Figure 8. In this setup, MATLAB served as the primary driver script and called custom Python functions to interface with GNU Radio, which controlled a pair of USRPs. Our MATLAB script loads the autoencoder via the Open Neural Network Exchange (ONNX) framework with a batch size of 1 and initializes the altimeter signal processor using the same parameters as in the data generation phase. Next, we launch the GNU Radio flowgraph, which is invoked from MATLAB through Python bindings and comprises two USRP sinks (transmitters) and one USRP source (receiver). In the OTA testbed, two USRP transmitters were used: one to transmit the clean FMCW radar chirp and another to transmit a high-power interfering signal. For the evaluation shown in Figure 8, the interfering signal was a QPSK-modulated

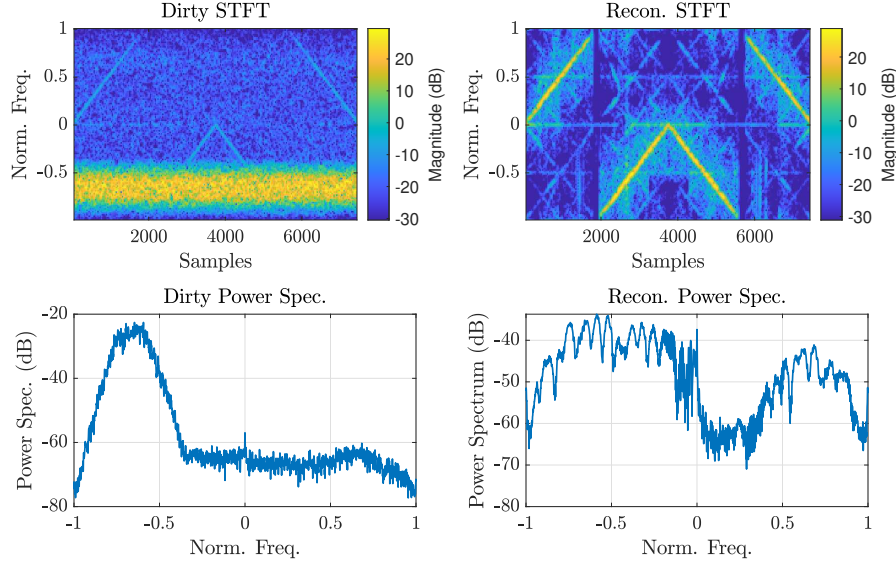


Fig. 9: Short-time Fourier transform and power spectrum for dirty and reconstructed over-the-air FMCW signals. A high-powered signal occupying 26.67% of the signal bandwidth is removed via the TCAE.

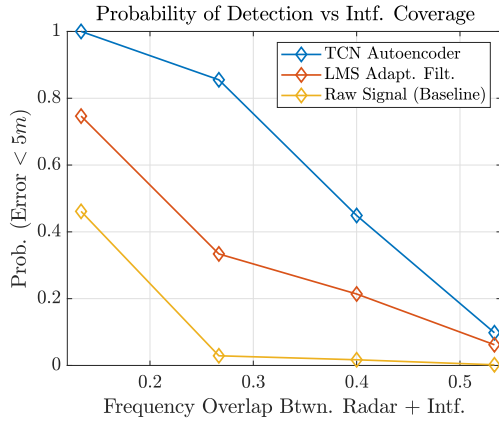


Fig. 10: Probability of correct ‘detection’ (where a detection corresponds to altitude error $< 5m$) vs overlap between FMCW and interfering signals evaluated on over-the-air data.

burst that temporally overlapped with the radar chirp and occupied approximately 26.7% of the radar bandwidth. The interference was designed to simulate a high-SIR challenge case, with power levels exceeding the radar return by up to 10 dB. The amount of temporal overlap between the radar chirp and interference was varied across evaluations to test model robustness. The overlap was defined as the fractional duration of the 7500-sample chirp during which the interfering signal was active. This scenario emulated a plausible airborne interference event, such as a communications signal from another nearby emitter operating in-band.

One sink transmits the clean FMCW signal of interest while the other transmits interference, and the USRP source captures the incoming signals, storing the IQ data in memory via a

GNU Radio vector sink. The MATLAB script then initiates an altimeter landing scenario loop by shifting the signal of interest to simulate changes in beat frequency similar to a radar approaching its target. After clearing the IQ data vector, the script pauses for 0.02 seconds to allow data accumulation before importing the data into MATLAB. We applied cross-correlation with the known reference chirp to segment the received IQ data into individual frames for autoencoder processing. Finally, the autoencoder outputs are processed by the radar altimeter processor to estimate altitude from the denoised signals, and we evaluate the model’s performance using RMSE across approximately 10 to 20 processed signals at each synthetic altitude.

The over-the-air tests further reinforce the performance observed in simulation. As shown in Figure 9, the TCN autoencoder successfully removes a high-powered interference signal occupying over 25% of the FMCW bandwidth while preserving the underlying radar return. Figure 10 shows a high probability of correct detection (defined by $< 5m$ error) across a range of interference overlaps, demonstrating robustness to challenging real-time conditions. These results confirm that the proposed approach can generalize to practical OTA scenarios and suggest feasibility for real-world altimeter operation.

VII. CONCLUSION AND FUTURE WORK

We have presented a robust approach to interference mitigation for radar altimeters using a temporal convolutional autoencoder. Our work integrated advanced deep learning techniques with a comprehensive radar simulation environment based on the MATLAB FMCW Radar Altimeter Simulation framework. The proposed TCN AEC demonstrated improved performance in preserving critical signal features, reducing interference, and providing accurate altitude estimates. Extensive simulation

studies, including evaluations on both MATLAB-generated and over-the-air data, show that the TCN model consistently outperforms conventional CNN and FC architectures in terms of quantitative metrics such as RMSE and qualitative assessments of range response.

The successful over-the-air evaluation using USRP hardware and real-time processing confirms that the proposed approach is not only effective in simulation but also viable under practical operating conditions. These findings provide a strong foundation for future testing aboard aircraft and further integration into radar altimeter systems.

A key advantage of our approach is the efficient design of the TCN architecture. By leveraging smaller kernel sizes, dilated convolutions, and carefully optimized hyperparameters, our model achieves faster per-epoch training and reduced parameter overhead. This computational efficiency makes the TCN-based solution well-suited for real-time hardware implementation, a critical factor for deployment in safety-critical aviation systems. Moreover, the ability of the autoencoder to learn a compact representation of the desired signal while effectively suppressing a wide range of interference types highlights its potential for adaptation to increasingly congested RF environments.

In addition to the technical contributions, our work has important implications for regulatory compliance and system safety. As commercial altimeter systems continue to face challenges from emerging communication signals, our interference mitigation strategy offers a promising solution to enhance reliability and maintain operational integrity. Future work will focus on further refining the model, exploring alternative network architectures, and extending the approach to other radar applications. Additional studies could also investigate the integration of our deep learning framework with advanced adaptive filtering techniques to further enhance performance under extreme interference conditions.

Overall, this work not only demonstrates the feasibility of deep learning-based interference mitigation for radar altimeters but also sets the stage for future research in this critical area. The proposed TCN AEC represents a significant step forward in ensuring the safe and reliable operation of radar altimeters in diverse and challenging environments.

REFERENCES

- [1] S. B. Brown, S. Young, A. Wagenknecht, D. Jakubisin, C. E. Thornton, A. Orndorff, and W. C. Headley, "Aircraft radar altimeter interference mitigation through a cnn-layer only denoising autoencoder architecture," in *Proc. IEEE MILCOM*, Oct. 2024.
- [2] T. Oyedare, V. K. Shah, D. J. Jakubisin, and J. H. Reed, "Interference suppression using deep learning: Current approaches and open challenges," *IEEE Access*, vol. 10, pp. 66 238–66 266, 2022.
- [3] C. Aydogdu, M. F. Keskin, G. K. Carvajal, O. Eriksson, H. Hellsten, H. Herbertsson, E. Nilsson, M. Rydstrom, K. Vanas, and H. Wymeersch, "Radar interference mitigation for automated driving: Exploring proactive strategies," *IEEE Signal Processing Magazine*, vol. 37, no. 4, pp. 72–84, 2020.
- [4] O. Kenneth, "Assessing 5g radar altimeter interference for realistic instrument landing system approaches," REMCOM, Tech. Rep., 2022.
- [5] RTCA, "Assessment of c-band mobile telecommunications interference impact on low range radar altimeter operations," RTCA, Tech. Rep., 2020.
- [6] A. Amaireh and Y. Zhang, "Machine learning-based identification and mitigation of 5g interference for radar altimeters," *IEEE Access*, 2024.
- [7] J. Rock and Y. Wang, "Radar altimeter coexist design in the 4.2–4.4 ghz band for multistage interference risk mitigation in 5g and beyond," *IEEE Aerospace and Electronic Systems Magazine*, vol. 39, no. 10, pp. 4–16, 2024.
- [8] S. Kokalj-Filipovic, R. Miller, and J. Morman, "Autoencoders for training compact deep learning rf classifiers for wireless protocols," in *2019 IEEE 20th International Workshop on Signal Processing Advances in Wireless Communications (SPAWC)*, 2019, pp. 1–5.
- [9] J. Fuchs, A. Dubey, M. Lübke, R. Weigel, and F. Lurz, "Automotive radar interference mitigation using a convolutional autoencoder," in *2020 IEEE International Radar Conference (RADAR)*, 2020, pp. 315–320.
- [10] S. Chen, J. Taghia, T. Fei, U. Kühnau, N. Pohl, and R. Martin, "A dnn autoencoder for automotive radar interference mitigation," in *ICASSP 2021 - 2021 IEEE International Conference on Acoustics, Speech and Signal Processing (ICASSP)*, 2021, pp. 4065–4069.
- [11] C. Lea, R. Vidal, A. Reiter, and G. D. Hager, "Temporal convolutional networks: A unified approach to action segmentation," 2016. [Online]. Available: <https://arxiv.org/abs/1608.08242>
- [12] S. Chauhan, Sehaj, S. Kumar, Siddharth, D. Panwar, and S. Chopra, "Temporal convolutional network and its application in various sectors," in *2023 3rd Asian Conference on Innovation in Technology (ASIAN-CON)*, 2023, pp. 1–7.
- [13] J. Park, Y. Park, and C.-I. Kim, "Tcae: Temporal convolutional autoencoders for time series anomaly detection," in *2022 Thirteenth International Conference on Ubiquitous and Future Networks (ICUFN)*, 2022, pp. 421–426.
- [14] H. Griffiths, L. Cohen, S. Watts, E. Mokole, C. Baker, M. Wicks, and S. Blunt, "Radar spectrum engineering and management: Technical and regulatory issues," *Proceedings of the IEEE*, vol. 103, no. 1, pp. 85–102, 2015.
- [15] F. Uysal and S. Sanka, "Mitigation of automotive radar interference," in *2018 IEEE Radar Conference (RadarConf18)*, 2018, pp. 0405–0410.
- [16] S. Bai, J. Z. Kolter, and V. Koltun, "An empirical evaluation of generic convolutional and recurrent networks for sequence modeling," 2018. [Online]. Available: <https://arxiv.org/abs/1803.01271>
- [17] MathWorks, "Fmcw radar altimeter simulation," 2024. [Online]. Available: <https://www.mathworks.com/help/radar/ug/fmcw-radar-altimeter-simulation.html>